Optical Studies of Pre-breakdown Electron Avalanches*

H. A. Blevin and J. Fletcher

School of Physical Sciences, Flinders University of South Australia,
Bedford Park, S.A. 5041, Australia.

Abstract

This paper reviews the work carried out at Flinders University over a number of years in relation to the light output from pre-breakdown Townsend discharges and isolated electron swarms. This 'luminous flux' technique has important advantages over conventional current measurements since regions remote from electrode boundaries can be studied yielding values of electron drift velocity, diffusion coefficients and ionisation/attachment rates from a single experiment. For the first time the internal structure of a single swarm has been studied by observing the light from different excited states. From these results it is clear that, in many cases, the diffusion equation does not give an adequate description of the spatial and temporal development of electron concentration, and higher order transport parameters are required in the analysis of experiments.

1. Introduction

The light emitted from established discharges and plasmas is of practical importance and has often been used for diagnostic purposes. However, there have been relatively few studies of the emission from Townsend discharges or drifting electron swarms. Costa (1939, 1940) and Geballe (1944) used subsidiary electrode systems to detect the presence of ultraviolet photons and assess their role in the production of secondary electrons. Measurements of excitation rates have been made by a number of workers (e.g. Corrigan and von Engel 1985; Legler 1963; Tachibana and Phelps 1979), while the first Townsend ionisation coefficient α_T has been observed by measuring the spatial distribution of light output from steady-state Townsend discharges (Buursen *et al.* 1972; Jelenkovic and Phelps 1986; Makabe *et al.* 1984). Raether (1963) and co-workers used both optical and electrical time resolved measurements to study electron avalanches and sequences of avalanches produced by secondary electrons. Breare and von Engel (1964) developed single photon counting techniques with both time and spatial resolution which were used to measure the electron drift velocity W in molecular hydrogen. The measurement of Wagner *et al.* (1967) indicated that electron diffusion was a tensorial quantity. This was placed on sound

---

theoretical basis by Skullerud (1969) and Parker and Lowke (1969). Similar behaviour had been observed previously in the motion of ion swarms and explained by Wannier (1953). These theories showed that the energy distribution function in an isolated electron swarm was not independent of position and as a consequence electron reaction rates would be spatially dependent. This discovery, together with the possibility of using the technique developed by Breare and von Engel (1964) to explore their internal structure, was the motivating force behind the studies which began at Flinders University in 1973.

Spatial variations in the electron velocity distribution can be represented by an expansion in terms of gradients in the electron concentration $n(\mathbf{r}, t)$:

$$f(\mathbf{v}, \mathbf{r}, t) = n(\mathbf{r}, t)g^0(\mathbf{v}) - \frac{\partial n}{\partial(\lambda_L z)}g^1(\mathbf{v}) + \frac{\partial^2 n}{\partial(\lambda_L z)^2}g^2(\mathbf{v}) - \dots, \qquad (1)$$

where it is assumed that $\mathbf{E}$ is constant in the negative z-direction and λ_L ($= W/2D_L$ where D_L is the longitudinal diffusion coefficient) is of the order of the reciprocal of the energy exchange distance. Terms involving radial gradients of n have been neglected in equation (1) as they are generally less important than those included. Alternatively the energy distribution function can be written as

$$f(\epsilon, \mathbf{r}, t) = n(\mathbf{r}, t)g^0(\epsilon) - \frac{\partial n}{\partial(\lambda_L z)}g^1(\epsilon) + \frac{\partial^2 n}{\partial(\lambda_L z)^2}g^2(\epsilon) - \dots. \qquad (2)$$

The continuity equation is

$$\frac{\partial n}{\partial t} + \nabla \cdot \mathbf{J} = n(\nu_i - \nu_a),$$

where the electron flux $\mathbf{J}(\mathbf{r}, t) = \int \mathbf{v}f(\mathbf{v}, \mathbf{r}, t)dv$ and ν_i, ν_a are the ionisation and attachment frequencies. Using the gradient expansion to determine $\mathbf{J}$ and ν_i (we will neglect attachment in the following discussion), then (Blevin and Fletcher 1984)

$$\frac{\partial n}{\partial t} + \left(W^0\frac{\partial n}{\partial z} - D^0\frac{\partial^2 n}{\partial x^2} - D^0\frac{\partial^2 n}{\partial y^2} - D_L'\frac{\partial^2 n}{\partial z^2} + S'\frac{\partial^3 n}{\partial z^3} - \dots\right)$$

$$= n\nu_i^0 - \frac{\nu_i^1}{\lambda_L}\frac{\partial n}{\partial z} + \frac{\nu_i^2}{\lambda_L^2}\frac{\partial^2 n}{\partial z^2} - \dots \qquad (3)$$

or

$$\frac{\partial n}{\partial t} + \left(W\frac{\partial n}{\partial z} - D_T\frac{\partial^2 n}{\partial x^2} - D_T\frac{\partial^2 n}{\partial y^2} - D_L\frac{\partial^2 n}{\partial z^2} + S\frac{\partial^3 n}{\partial z^3} - \dots\right) = n\nu_i^0. \qquad (4)$$

Here $W = W^0 + \nu_i^1/\lambda_L$, and $D_L = D_L' + \nu_i^2/\lambda_L^2$ are the electron drift velocity and longitudinal diffusion coefficient respectively. Equation (4) is the usual starting

point for analysis of swarm experiments and is usually truncated at second order derivatives to give the diffusion equation,

$$\frac{\partial n}{\partial t} + \left(W\frac{\partial n}{\partial z} - D_T\frac{\partial^2 n}{\partial x^2} - D_T\frac{\partial^2 n}{\partial y^2} - D_L\frac{\partial^2 n}{\partial z^2} \right) = n\nu_i^0 \,. \tag{5}$$

It is important to realise that the term in parentheses no longer represents the divergence of the electron flux although it is almost universal practice to calculate electron currents at electrodes from W and D_L. The resultant errors can be large ($\geq 10\%$ in nitrogen at $E/N = 500$ Td) when ionisation (or attachment) are present (Kelly and Blevin 1989).

Experiments utilising the luminous flux technique do not measure $n(\mathbf{r}, t)$ directly, but observe the photon production rate

$$n_{ph}(\mathbf{r}, t) = \frac{1}{\tau}\int_0^t n(\mathbf{r}, t')\nu_{ex}(\mathbf{r}, t')e^{-(t-t')/\tau}dt' \,, \tag{6}$$

where τ is the lifetime of the excited state and ν_{ex} is the excitation frequency for that state, although more complicated expressions are required for more than one decay channel and cascading contributes to the population of the state (Wedding et al. 1985).

The excitation rate can be obtained from the gradient expansion of the energy distribution function, equation (2), and the appropriate excitation cross sections:

$$n(\mathbf{r}, t)\nu_{ex}(\mathbf{r}, t) = n(\mathbf{r}, t)\int g^0(\epsilon)\nu_{ex}(\epsilon)d\epsilon - \frac{\partial}{\partial(\lambda_L z)}\int g'(\epsilon)\nu_{ex}(\epsilon)d\epsilon + \dots$$

$$= n(\mathbf{r}, t)\nu_{ex}^0 - \frac{\partial n}{\partial(\lambda_L z)}\nu_{ex}^1 + \frac{\partial^2 n}{\partial(\lambda_L z)^2}\nu_{ex}^2 - \dots \,. \tag{7}$$

The studies of swarms and established discharges in our laboratories have been directed mainly towards a better understanding of the various terms in equations (4) and (7). This work has demonstrated the importance of the skewness coefficient S in describing swarm behaviour and for the first time direct evidence of spatial variations in the energy distribution have been observed by analysing radiation from different excited states using equations (6) and (7). In the course of these investigations transport parameters, ionisation rates and lifetimes of excited states (and in some cases, collisional quenching rates) have been measured for a number of gases. These data will not be emphasised in this review and we concentrate mainly on concepts of general applicability. In Section 2 our studies of steady-state discharges will be described, including the boundary layer regions near the cathode and anode. Experiments using isolated swarms are described in Section 3, while a discussion is given of some experiments involving secondary electron production at the cathode and subsequent avalanches. All this work was supplemented by Monte Carlo simulations since these give definitive results free from the various truncations involved in a practical utilisation of equations (4) and (7).

The experiments were carried out using several different discharge vessels. However, they were of similar construction to that shown schematically in Fig. 1.

The electrode spacings were typically from 2 to 10 cm and electrons from the thermionic source could be admitted to the drift region either continuously or in a pulsed mode by appropriate gating of the bias voltage on the dispenser cathode. Photons emitted from the discharge entered a collimator, wavelength selector (monochromator or interference filter) and photomultiplier, so that the photons emitted along the line of sight of the collimator could be detected with spatial and time resolution as required. A tubular collimator provided both transverse and longitudinal scans of the drift region while a slit collimator integrated counts over all radial positions, effectively reducing the discharge to a one dimensional geometry.
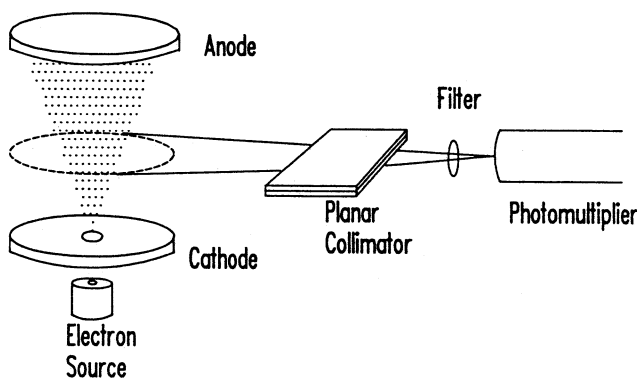

Fig. 1.   Schematic of the basic electrode assembly used in the present work. A slit collimator is shown but a cylindrical collimator was often used.

2.   Steady-state Townsend Discharges

If the light output from a steady-state discharge is observed as a function of axial position using the slit collimators then three distinct regions are indicated; the cathode and anode boundary layers and an intermediate region where the energy distribution function is no longer dependent on the initial electron energy distribution. In this central region the radially integrated energy distribution function is independent of axial position and in the presence of ionisation both the electron concentration and light output grow exponentially as $\exp(\alpha_T z)$, where α_T is the first Townsend ionisation coefficient. An example of such a scan is shown in Fig. 2 for nitrogen gas with $E/N = 555$ Td (N is the neutral gas concentration) at a pressure of $0\cdot12$ Torr and an electrode separation of $d = 3\cdot6$ cm. Radiation from the $C^3\pi_u \to B^3\pi_g(0,0)$ transition at $337\cdot1$ nm and from the $B^2\sum_u^+ \to X^2\sum_g^+(0,0)$ transition at $391\cdot4$ nm are shown.

(a)   Cathode Boundary Region

The detailed structure of the discharge in this layer is sensitive to the initial energy distribution of the source electrons (Kelly *et al.* 1989). However, for electrons injected into the drift region with energies ≈ 5–10 eV the oscillations in luminosity shown for the $337\cdot1$ nm radiation in Fig. 2 are a striking feature of the measurements in N_2. Monte Carlo simulations show that the large fluctuations in light output are accompanied by variations in electron concentration and mean

energy. Although only two or three peaks in light output are seen in N_2, the phenomenon is closely related to the more numerous luminous layers seen in rare gas discharges (Holst and Oosterhuis 1921). Experiments in the rare gases carried out in these laboratories (Fletcher 1985; Fletcher and Purdie 1987) together with detailed Monte Carlo simulations for neon show that the structure of the discharge in the cathode non-equilibrium region is very sensitive to the cross sections for the first few excited states. It has been suggested that a more detailed study of radiation from the cathode non-equilibrium region could play a more important role in evaluation of cross section data (Kelly *et al.* 1989).
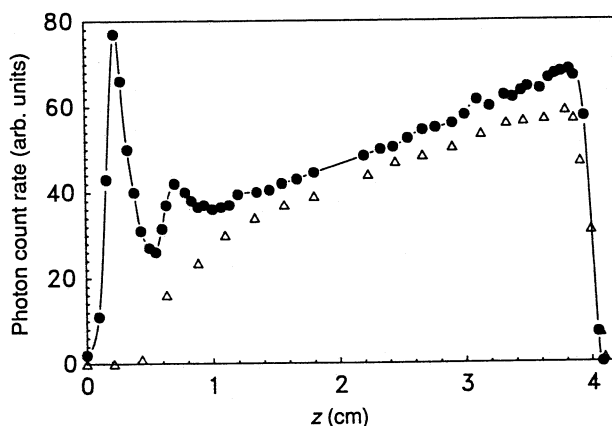

Fig. 2. The photon count rate as a function of axial distance from the cathode z for nitrogen: $E/N = 555$ Td; $p_0 = 0 \cdot 12$ Torr; wavelength, ● — $337 \cdot 1$ nm, △ — $391 \cdot 4$ nm.

(b) Anode Boundary Region

This region extends back from the anode for a distance of the order of two energy exchange distances. For an absorbing anode, the reduction of backscattered electrons produces a sharp decrease in electron concentration as the anode is approached. Since these absorbed electrons would otherwise lose energy in moving along the field, their absence reduces mainly the low energy part of the energy distribution and hence the mean energy increases towards the anode. A Monte Carlo investigation (Kelly and Blevin 1989) confirmed that the electron flux to the anode is not given by the parameters W and D_L but the flux related parameters W^0 and D'_L as discussed in the Introduction. These parameters have not been measured experimentally when ionisation and/or attachment are present. Moreover, experiments (Blevin *et al.* 1987) show that the structure of the anode region is sensitive to the anode surface material, indicating that reflected electrons and secondary electron production at the anode are important. These considerations lead to the conclusion that it is not possible to relate the measured electron current at the anode to electron concentrations in the body of the discharge unless a detailed account of the process acting at the boundary is included in the analysis.

(c) 'Equilibrium' Region

The energy distribution function in the central region of the discharge is not strictly in equilibrium since spatial gradients in concentration occur and these depend upon the source geometry as well as the E/N value. Only for the radially integrated distribution function where $n(z) \propto \exp(\alpha_T z)$ does the expression in equation (2) yield a distribution function $f(\epsilon, z, t)$ which, when normalised, is z-independent. Consequently the radially integrated light output is proportional to $n(z)$ and its axial dependence gives a measure of the first Townsend ionisation coefficient. Measurements of D_T/μ in N_2 have been made by Fletcher and Reid (1980) and by Wedding *et al.* (1985) by taking lateral scans across the discharge with the tubular collimator and assuming that the light output is proportional to the electron concentration integrated along the line of sight. In view of the following discussion this is not strictly correct and there may be systematic errors in the derived D_T/μ values. Nevertheless, the results obtained by the luminous flux method are within the combined experimental errors of values obtained by the Townsend–Huxley method, which measures the current distribution at the anode (Roznerski *et al.* 1990).
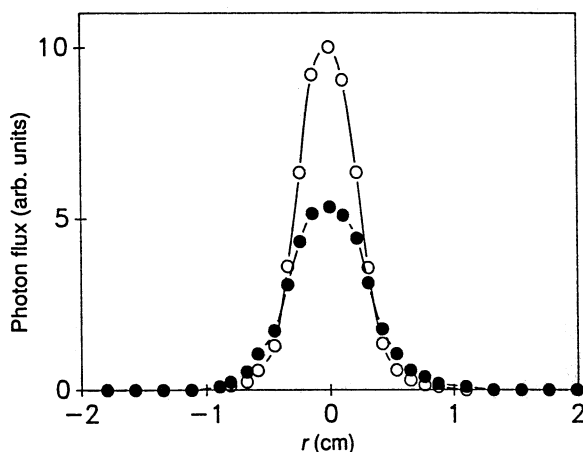

Fig. 3. Photon flux as a function of radial distance across a discharge in $CO_2 : N_2 : He : CO$ (6:34:54:6) mixture: $\bigcirc$ — 337·1 nm; $\bullet$ — 391·4 nm, for $E/N = 300$ Td, $_p0 = 0·373$ Torr, $z = 0·4$ cm.

In a three dimensional steady-state Townsend discharge the gradients

$$\partial n(r, z)/\partial(\lambda_L z), \ \partial^2 n(r, z)/\partial(\lambda_L z)^2, \ ...$$

are radially varying quantities so that equation (2) shows that the energy distribution function is a function of radial position at a fixed z-value. This spatial variation in the distribution function was confirmed by observing the 337·1 and 391·4 nm radiation from discharges in a $CO_2 : N_2 : He : CO$ (6:34:54:6) gas mixture. Abel inversion of the integrated line of sight data showed a strong radial dependence in the ratio of excited state populations (Wedding and Kelly 1989). An example of the radial dependence of these emissions is shown in Fig. 3. It was subsequently shown (Blevin and Kelly 1990) that at least second order

derivatives are required in the gradient expansion (equation 2) to give satisfactory agreement with the observations.

Discharges in transverse magnetic fields have also been studied using the luminous flux technique and the results compared with Monte Carlo simulations (Brennan *et al.* 1990; Brennan and Garvie 1990; Garvie and Brennan 1990). Again spatial variations in the electron energy distribution were evident and in general agreement with the gradient expansion appropriate to $\mathbf{E} \times \mathbf{B}$ discharges. Measured transport parameters in $\mathbf{E} \times \mathbf{B}$ discharges in N_2 differed from Monte Carlo simulation results even though the cross sections gave good agreement with experimental values in the absence of the magnetic field. This raises some doubt concerning the accuracy of the cross section set, although the experiments were of limited accuracy, and there is a need for additional experiments to confirm and extend the present results. Since $\mathbf{E} \times \mathbf{B}$ discharges are not cylindrically symmetric, tomographic reconstructions were required to determine spatial variations in excitation rates and this leads to complexities in the experimental design.
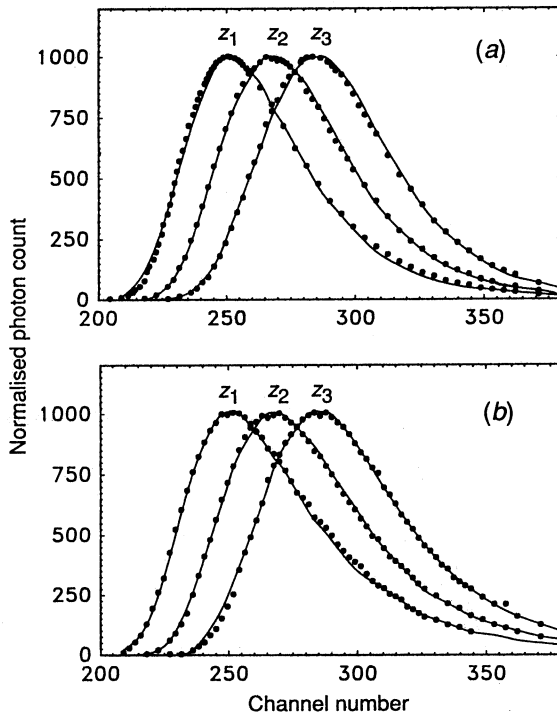

Fig. 4. Normalised photon distributions in nitrogen: (*a*) $337 \cdot 1$ nm (*b*) $391 \cdot 4$ nm. Here $E/N = 443$ Td, $p_0 = 0 \cdot 28$ Torr, $z_1 = 2 \cdot 2$ cm, $z_2 = 3 \cdot 2$ cm, $z_3 = 4 \cdot 3$ cm: $1 \cdot 714$ ns per channel. The curves are a theoretical fit using the gradient expansion terminated at the second derivative.

3. Pulsed Swarms

These experiments are by far the most productive in terms of providing information about the physics of isolated swarms. Since a steady-state discharge

can be regarded as a sequence of localised swarms it follows that a detailed understanding of individual swarms also leads to a full description of the steady-state. An example of the luminous flux technique applied to travelling swarms in N_2 gas for $E/N = 443$ Td, $p = 0 \cdot 28$ Torr is shown in Fig. 4. The photon count rate as a function of time after injection of the electrons is shown for the $337 \cdot 1$ and $391 \cdot 4$ nm bands at three axial positions, $z_1 = 2 \cdot 2$ cm, $z_2 = 3 \cdot 2$ cm and $z_3 = 4 \cdot 3$ cm. The slit collimators were used in this experiment (Kelly 1990) so that the theory for a one-dimensional discharge is appropriate. The curves are the best theoretical fits to the data using equation (4) (in one-dimensional form but truncated at third order derivatives) and equations (6) and (7). Equation (6) is modified to allow for population of the $C^3 \pi_u$ state by collisional deactivation of the $E^3 \sum_g^+$ state and equation (7) was truncated at second order derivatives of the electron concentration. A multi-parameter least squares fitting procedure yields values of $W, D_L, S, \nu_i^0, \nu_{ex}^1/\nu_{ex}^0, \nu_{ex}^2/\nu_{ex}^0$ and the lifetimes of the excited states which in some cases are pressure dependent due to collisional quenching. Absolute values of the excitation frequencies were not obtained since the electron concentration in the discharge is not known (cf. Section 2c).

A Monte Carlo study (Blevin and Kelly 1991) of travelling swarms in N_2 at $E/N = 332$, 443 and 511 Td showed that it is necessary to include skewness
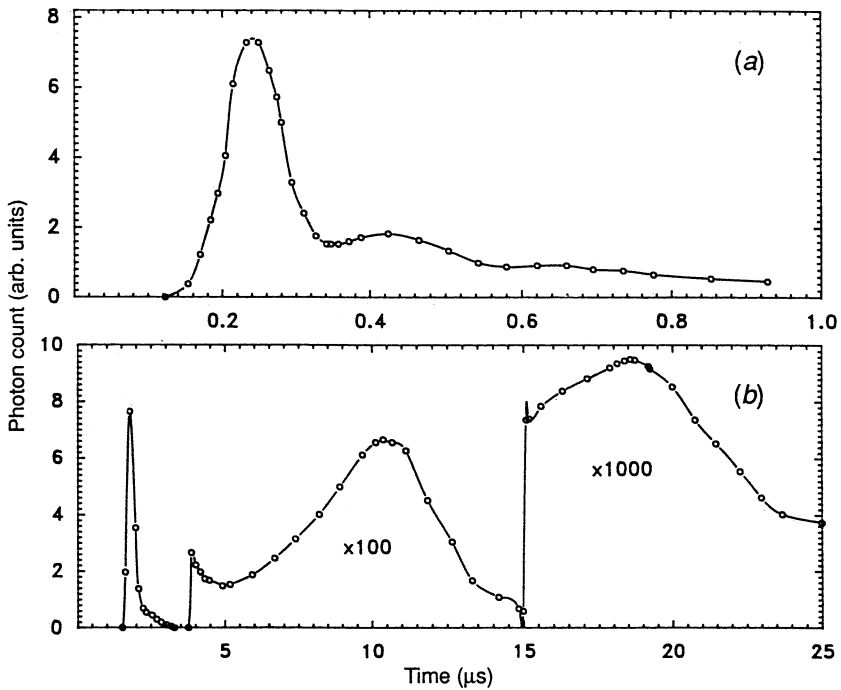

Fig. 5. Photon flux as a function of time in a hydrogen discharge for $E/N = 298$ Td: (a) Short time scale showing photoelectron-produced secondary avalanches. (b) Long time scale showing ion-produced secondary peaks.

in the continuity equation, although even higher order transport parameters are required for times less than about ten energy exchange times from the time of the initiating pulse. For these E/N values, the excitation rate to the $C^3\pi_u$ state was adequately described by the first order gradient expansion in equation (7), while the excitation rate to the $B^2\sum_u^+$ state required higher order gradients.

These experiments clearly demonstrate the variations in electron mean energy throughout the swarm with excitation to the $B^2\sum_u^+$ state (with a higher threshold excitation energy) occurring preferentially at the front of the swarm where the mean energy is higher (Blevin and Kelly 1991).

4. Secondary Electron Production

As the Nd product is increased and breakdown of the gap is approached, the total production of photons, positive ions and (in some gases) metastable atoms increases rapidly and produces secondary electron emission from the cathode. These secondary electrons produce further sequences of avalanches which can be detected by the luminous flux method (Fletcher and Blevin; 1981 Amies and Fletcher 1983). The light output observed at a fixed collimator position as a function of time is shown in Fig. 5 for a discharge in H_2 for $E/N = 298$ Td ($p = 0\cdot5$ Torr, $d = 10$ cm). Fig. 5a shows a sequence of secondary avalanches produced by photoelectric emission spaced by approximately one electron transit time. On a longer time scale Fig. 5b shows a sequence of avalanches spaced by approximately one ion transit time. These avalanches are partly produced by positive ion induced secondary electron emission but photoelectric emission is also present and accounts for about 50% of the total count as indicated by the short time scale results shown in Fig. 5a.

The time dependence of the positive ion induced emission can be calculated from the ion flux to the cathode, $D_i\partial n_i(z,t)/\partial z\ |_{z=0}$, where D_i is the ion longitudinal diffusion coefficient and $n_i(z,t)$ is the positive ion concentration given
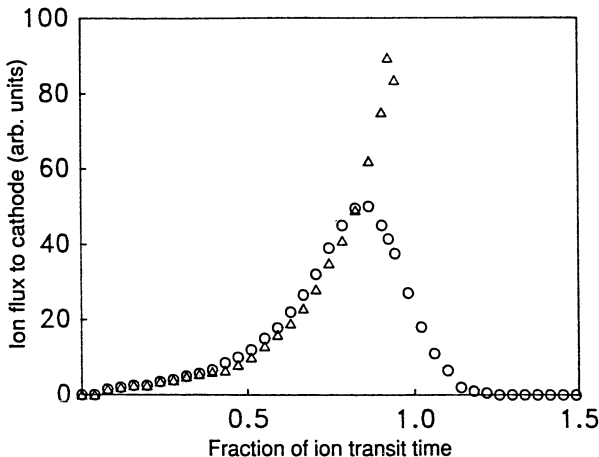

Fig. 6. Calculated ion flux to the cathode during the first $1\cdot5$ ion transit times in hydrogen. The experimental conditions are as in Fig. 5. $\triangle$ — neglecting ion diffusion; $\bigcirc$ — including ion diffusion. The general shape is similar to that observed in hydrogen experiments (Fig. 5).
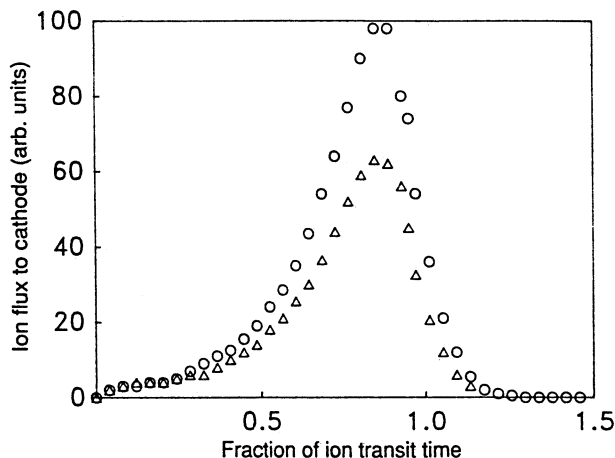
Fig. 7. Calculated ion flux to the cathode for the first $1 \cdot 5$ ion transit times in nitrogen: $\bigcirc$ — with diffusion; $\triangle$ — including the ion reaction, $N^+ + 2N_2 \rightarrow N_3^+ + N_3$. The flux is seen to drop rapidly to zero after one transit time while the experimental data in nitrogen show a large 'tail' after each ion transit time.

by Purdie and Fletcher (1989). Fig. 6 shows the results for approximately the same conditions applicable to the experimental results in Fig. 5. The calculated results are also shown when ion diffusion is neglected and clearly diffusion must be included in order to give an adequate explanation of the time dependence of the secondary emission. In a series of experiments Fletcher and Blevin (1981) showed that the positive ions responsible for secondary electron emission in H_2 discharges were the atomic H^+ ions produced by dissociative ionisation of the molecule. They also concluded that the atomic ion was responsible for the secondary electron production in N_2 discharges, as judged by the transit time of ions drifting across the gap. However, the time dependence of the ion-induced secondary emission in N_2 did not follow the expected trend shown by the experiments in H_2 (Fig. 5) or the calculated values (Fig. 6). The peak emission occurs somewhat earlier than the N^+ ion transit time and is followed by a slowly decreasing 'tail'. Similar trends are evident in the work of Gylys *et al.* (1989) at very high E/N values. It was thought that ion reactions may distort the arrival time distribution of ions at the cathode, so that the removal of atomic ions by the reaction $N^+ + 2N_2 \rightarrow N_3^+ + N_2$ was included in calculations of the ion flux to the cathode. Reaction rates given by Mosley *et al.* (1969) were used to calculate the ion flux to the cathode for a variety of conditions and a typical result is shown in Fig. 7. None of our calculations showed the tail in the arrival time distribution. It is possible that this could be provided by the reverse reaction with N_3^+ ions and the neutral gas or perhaps other ions contribute partially to secondary electron production in nitrogen discharges. There is clearly a need for further work, combining measurements of secondary electron emission (using the luminous flux technique) and arrival time spectra of mass-identified ions.

5. Conclusion

From the photon flux work described above it is apparent that most of the electron transport coefficients, e.g. W, ND_L, ND_T, and reaction rates, e.g. α/N, have been measured with a high degree of accuracy in hydrogen, nitrogen and the rare gases. It is equally apparent that, at present, the behaviour of the C state radiation in nitrogen is not fully understood. For example, available cross sections used in a Monte Carlo simulation yield excitation reaction rates approximately 50% of the observed values. Similarly, whilst secondary electron data in hydrogen are consistent with the suggested theory, in nitrogen the shape of the time resolved ion-produced secondary electron curves cannot be fully explained.

Acknowledgments

References

Amies, B. W., and Fletcher, J. (1983). *J. Phys.* D **16**, L133.
Blevin, H. A., Brennan, M. J., and Kelly, L. J. (1987). Eighteenth Int. Conf. on Phenomena in Ionised Gases, Vol. 1 (Ed W. T. Williams), p. 92 (Hilger: London).
Blevin, H. A., and Fletcher, J. (1984). *Aust. J. Phys.* **37**, 593.
Blevin, H. A., and Kelly, L. J. (1990). 'Nonequilibrium Effects in Ion and Electron Transport' (Plenum: New York).
Blevin, H. A., and Kelly, L. J. (1991). 'Gaseous Electronics and its Applications', p. 127 (KTK: Tokyo).
Breare, J. M., and von Engel, A. (1964). *Proc. R. Soc. London* A **282**, 390 .
Brennan, M. J., and Garvie, A. M. (1990). *Aust. J. Phys.* **43**, 765.
Brennan, M. J., Garvie, A. M., and Kelly, L. J. (1990). *Aust. J. Phys.* **43**, 27.
Buursen, C. G. J., de Hoog, F. J., and van Mortfort, L. H. (1972). *Physica* **60**, 244.
Corrigan, S. J. B., and von Engel, A. (1985). *Proc. R. Soc. London* A **245**, 335.
Costa, H. (1939). *Z. Phys.* **113**, 531.
Costa, H. (1940). *Z. Phys.* **116**, 508.
Fletcher, J. (1985). *J. Phys.* D **18**, 221.
Fletcher, J., and Blevin, H. A. (1981). *J. Phys.* D **14**, 27.
Fletcher, J., and Purdie, P. H. (1987). *Aust. J. Phys.* **40**, 383.
Fletcher, J., and Reid, I. (1980). *J. Phys.* D **13**, 2275.
Garvie, A. M., and Brennan, M. J. (1990). *Aust. J. Phys.* **43**, 779.
Geballe, R. (1944). *Phys. Rev.* **66**, 316.
Gylys, V. T., Jelenkovic, B. M., and Phelps, A.V. (1989). *J. Appl. Phys.* **65**, 3369.
Holst, G., and Oosterhuis, E. (1921). *Physica* **1**, 78.
Jelenkovic, B. M., and Phelps, A. V. (1986). *Bull. Am. Phys. Soc.* **31**, 152.
Kelly, L. J. (1990). Ph.D. Thesis, Flinders University.
Kelly, L. J., and Blevin, H. A. (1989). Nineteenth Int. Conf. on Phenomena in Ionised Gases, Vol. 4. (Ed. J. M. Labut), p. 892 (Univ. of Belgrade).
Kelly, L. J., Brennan, M. J. and Wedding, A. B. (1989). *Aust. J. Phys.* **42**, 365.
Legler, W. (1963). *Z. Phys.* **173**, 169.

Makabe, T., Awai, H., and Mori, T. (1984). *J. Phys.* D **17**, 2367

Mosley, J. T., Snuggs, R. M., Martin, D. W., and McDaniel, E. W. (1969). *Phys. Rev.* **178**, 240.

Parker, J. H., and Lowke, J. J. (1969). *Phys. Rev.* **181**, 290.

Purdie, P. H., and Fletcher, J. (1989). *J. Phys.* D **22**, 759.

Raether, H. (1963). 'Electron Avalanches and Breakdown' (Butterworths: London).

Roznerski, W., Mechlinska-Drewko, J., and Leja, K. (1990). *J. Phys.* D **23**, 1461.

Skullerud, H. R. (1969). *J. Phys.* B. **2**, 696.

Tachibana, K., and Phelps, A.V. (1979). *J. Chem. Phys.* **71**, 3544.

Wagner, E. G., David, F. J., and Hurst, G. S. (1967). *J. Chem. Phys.* **47**, 3138.

Wannier, G. H. (1953). *Bell Syst. Tech. J.* **32**, 170.

Wedding, A. B., Blevin, H. A., and Fletcher, J. (1985). *J. Phys.* D **18**, 2361.

Wedding, A. B., and Kelly, L. J. (1989). *Aust. J. Phys.* **42**, 101.